



Contents lists available at ScienceDirect

Arabian Journal of Chemistry

journal homepage: www.ksu.edu.sa

Multi-physical and anti-corrosion properties of graphene-reinforced epoxy nanocomposite coatings for industrial applications

Md. Ramjan Ali^{a,*}, Mohammad Asaduzzaman Chowdhury^a, Mohammad Shahin^a,
Md. Mostafizur Rahman^a, Md. Osman Ali^a, Md. Abdul Gafur^b

^a Department of Mechanical Engineering, Dhaka University of Engineering & Technology, Gazipur 1707, Bangladesh

^b Pilot Plant and Process Development Centre, Bangladesh Council of Scientific and Industrial Research, Dhaka 1205, Bangladesh

ARTICLE INFO

Keywords:

Graphene-reinforced epoxy nanocomposite coating
Corrosion
Surface roughness
Water absorptivity
Thermal stability
Electrical conductivity

ABSTRACT

Polymer-based coatings are widely used as a protective barrier to corrosion, but their performance is not sufficiently sustainable for industrial applications due to the formation of micropores and microcracks during solidification. Graphene is a promising reinforcing element acting as a filler for polymeric coatings. This study used 1–5 wt% graphene synthesized by the electrochemical exfoliation process as a reinforcing nanofiller to manufacture graphene-reinforced epoxy nanocomposite (GREN) coatings. Copper was used as a substrate material for coating with GREN by a bar coating method. GREN coatings were characterized by X-ray diffraction, Raman spectroscopy, FTIR spectroscopy, FESEM, and EDX. A comprehensive investigation was conducted on the various multi-physical properties of GREN coatings, including coating thickness, surface roughness, adhesiveness, surface wettability, water absorptivity, thermal stability, electrical conductivity, and anti-corrosion capabilities. The results exhibited that graphene fills micro-pores produced in epoxy during solidification. The surface roughness significantly decreased to 0.25 μm with the addition of 5 wt% graphene in pure epoxy. In addition, the adhesiveness, thermal stability, and electrical conductivity of GREN coatings increased with the increase in graphene content. The GREN coatings containing 3 wt% and 5 wt% graphene revealed hydrophobic surface showing 94° and 102° water contact angle, respectively. In the electrochemical analysis and immersion test in 3.5 % NaCl solution for 600 h, the GREN coatings showed higher corrosion resistance without compromising their electrical conductivity compared to the pure epoxy. Based on the results, GREN can be a promising coating material for aerospace, mining, and electronic packaging applications. Apart from this, the results of this work will explore the new significance in industry, where multi-physical properties from a single nanocomposite coating are crucial.

1. Introduction

Corrosion is a natural electrochemical process that causes massive global economic damages per year with progressive adverse effects on structural integrity, which results in disasters such as machinery breakdown and toxic release (Nahlé et al., 2022; Al-Moubaraki and Obot, 2021). Due to their significant energy consumption, low efficiency, and lack of sustainability, conventional approaches such as mechanical cleaning and de-rusting are inadequate in addressing these challenges. In earlier investigations, a variety of methods, including organic polymer coatings, hydrophobic coatings, self-cleaning coatings,

and composite coatings, were used to protect metals from corrosion (Zhu et al., 2023; Fadl et al., 2021). Recently, a multi-functional coating is one of the most cutting-edge approaches in the aerospace, automotive, marine, defense, and electronic industries (Jena and Philip, 2022; Xavier, 2023). This approach strongly prevents metal from corrosion as well as provides some additional properties such as electrical conductivity, thermal stability, hydrophobicity, antimicrobial capability, antifouling, and self-healing (Chowdhury et al., 2022; Ying et al., 2020; Zhang et al., 2022; Zhang et al., 2021). For instance, anti-corrosive and electrically conductive properties are required in coatings to avoid the formation of ice and anti-static safety for aircraft, anti-static grounding for power

Peer review under responsibility of King Saud University.

* Corresponding author.

E-mail addresses: ramjan@duet.ac.bd (Md.R. Ali), asad@duet.ac.bd (M.A. Chowdhury), shahin.duet37@gmail.com (M. Shahin), mostafizme@duet.ac.bd (Md.M. Rahman), osman@duet.ac.bd (Md.O. Ali), d_r_magafur@yahoo.com (Md.A. Gafur).

<https://doi.org/10.1016/j.arabjc.2023.105424>

Received 11 May 2023; Accepted 31 October 2023

Available online 3 November 2023

1878-5352/© 2023 The Authors. Published by Elsevier B.V. on behalf of King Saud University. This is an open access article under the CC BY license (<http://creativecommons.org/licenses/by/4.0/>).

systems, and electromagnetic shielding (EMI) for electronic devices (Li et al., 2023; Vovchenko et al., 2023; Pradhan et al., 2022).

The protective coatings must have excellent bonding strength, strong abrasion resistance, and superb anti-corrosive properties to have long-lasting protection (Bao et al., 2020). Organic polymeric coatings have become an essential alternative for the safety of metallic substrates by providing a physical barrier (Habib et al., 2021). Various kinds of polymers and their composites are used for the development of those coatings. Polymeric coatings such as epoxy are widely used for industrial applications because of their environmental stability, excellent metal adhesion, desirable electrical characteristics, and comparatively low cost (Wei et al., 2020; Dagdag et al., 2020). However, at the curing time, solvent evaporation causes the formation of micro-pores, which are entryways into the coating matrix for corrosive electrolyte penetration, leading to a decrease in hardness and anti-corrosion efficiency (Zehra et al., 2023). Including nanofillers in polymeric coatings enhances their mechanical, thermal, and corrosion resistance efficiency as they can block the micro-pores and cavities produced in the matrix during solidification (Pourhashem et al., 2020; Song et al., 2021). However, thermoset polymeric coatings are influenced by the process of network formation, wherein fillers can either facilitate or impede the curing reactions (Jouyandeh et al., 2019). The degree of curing or crosslinking of polymeric coatings in the presence of nanoparticles largely depends on the filler's shape, surface chemistry, and dispersion (Nonahal et al., 2018; Nonahal et al., 2018).

Recently, graphene has gained considerable interest from previous studies owing to its distinctive characteristics, which include a substantial specific surface area ($2630 \text{ m}^2/\text{g}$), significant thermal conductivity ($\sim 4000 \text{ W m}^{-1}\text{K}^{-1}$), high electrical conductivity ($\sim 3.4 \times 10^4 \text{ Sm}^{-1}$), and supreme tensile strength (130 GPa) (Zhang et al., 2022; Yahya et al., 2023). Moreover, graphene can be used in anticorrosive coating systems since it has more excellent barrier protection properties than bare metals (Zhang et al., 2021; Zhang et al., 2022). Furthermore, such a barrier period is only available for temporary applications due to inevitable defects such as single vacancy, line, multiple vacancy, and edge defects generated on its surface (Verma et al., 2023; Kwak et al., 2017). The use of graphene as a nanofiller in a polymer-based coating might be a potential approach to solve these issues as the graphene can block micro-pores and cavities of the polymer matrix as well as increase the crosslinking density during solidification (Jouyandeh et al., 2019; Yarahmadi et al., 2018).

A large number of polymer-based nanocomposite coatings have been reported that are widely utilized to prevent corrosion, including epoxy (Shi et al., 2023), polyurethane (Haghdadeh et al., 2018), polyaniline (Zhang et al., 2023), polystyrene (Bahgat Radwan et al., 2021), polypropylene (Zhang et al., 2021), poly (vinyl alcohol) (Jaseela et al., 2020), poly (methyl methacrylate) (Uvida et al., 2022) and so on. Xavier et al. (Xavier et al., 2021) reported TiC nanoparticles reinforced epoxy nanocomposite coatings on Mg alloy for the improvement of corrosion protection with superior hydrophobic and mechanical properties. Similarly, Kim et al. (Kim et al., 2019) investigated graphene/poly siloxane-based nanocomposite coatings on Cu substrate as an electrically conductive and anti-corrosive barrier. However, the results showed an insufficient level of hydrophobicity, electrical conductivity and corrosion resistance. In addition, the understanding of preventing corrosion of polymer-based nanocomposite coatings is still not clear, which strongly complements further extensive studies with polymer-based nanocomposite coatings.

Based on the above perspectives, the current research work aims to fabricate multi-functional graphene-reinforced epoxy nanocomposite (GREN) coatings to enhance corrosion resistance, maintaining their physical properties, including coating thickness, adhesiveness, surface roughness, surface wettability, water absorptivity, electrical conductivity, and thermal stability. This study provides a clear understanding of the effects of different parameters, including graphene contents as a reinforcing element and coating method, that will contribute to different

technologies, including food packaging, pharmaceuticals, chemical technology, and electronic devices.

2. Materials and method

2.1. Starting materials

Graphite foil (C > 99 %, size: 150 x 150 mm, thickness: 1.0 mm), sodium chloride (NaCl > 98 %), ammonium sulphate ($(\text{NH}_4)_2\text{SO}_4$ > 98.5 %), ethyl alcohol ($\text{CH}_3\text{CH}_2\text{OH}$), and acetone (CH_3COCH_3) were bought from Sinopharm Chemical Reagent Co. Ltd., China. Diglycidyl ether of bisphenol-A (DGEBA) epoxy resin (Lapox B-11) and unmodified aliphatic polyamine epoxy hardener (Lapox K-6) were purchased from Atul Ltd., Gujrat, India. A porous nylon membrane (pore size: 0.2 μm and dia.: 90 mm) was purchased from Whatman, Germany. Stainless steel rod (grade: 304, dia.: 12 mm), stainless steel tiny wire (cold drawn and annealed, dia.: 0.02 mm), and Cu foil (Cu > 99.99 %, thickness: 0.1 mm) were purchased from Saky Steel Co. Ltd. Shanghai, China. Silicon carbide emery paper (electro-coated, grit: 500 to 2000) was purchased from Orient Craft Ltd., India.

2.2. Synthesis of graphene

Two electrode systems were used to perform the electrochemical exfoliation of graphite. Working and counter electrodes were made of graphite foil and platinum wire, respectively, where 0.1 M molar aqueous $(\text{NH}_4)_2\text{SO}_4$ was used as electrolytic. After supplying a DC + 10 V, graphite foil was exfoliated into electrolytes, and then the exfoliated sheets were sonicated using a bath-sonicator for at least 2 h to convert as graphene nanosheets, which were then separated by vacuum filtering using a porous nylon membrane (Zhou et al., 2013).

2.3. Wire-wound metering rod and coating substrate preparation

A wire-wound metering rod, sometimes referred to as a Mayer rod, was manufactured using a lathe by utilizing a stainless steel (SS) rod measuring 12 mm in diameter and 455 mm in length, together with a miniature SS wire having a diameter of 0.02 mm. This rod was used to fabricate coating on metal substrate. Thin metal foil (copper) was used as the substrate in this study. The copper foil was cut into 12 cm x 6 cm pieces for each sample. After being coarse-grounded with silicon carbide sheets (1000 to 2000 grit), the substrates were ultrasonically cleaned with acetone and then washed in deionized water. The substrates were then mirror polished using a two-step materialographic grinding and polishing process with a 3 μm diamond polish suspension and a 0.5 μm alumina polish suspension, respectively. Finally, the polished substrates were ultrasonically cleaned and dried with a nitrogen (N_2) stream.

2.4. Fabrication of graphene-reinforced epoxy nanocomposite (GREN) coatings

Due to the hydrophobic nature of graphene nanosheets, it is complicated to disperse them within a polymer matrix. In this study, various amounts of 1, 2, 3, 4 and 5 wt% powder graphene was added with the required quantity of ethanol to make the graphene-ethanol solutions. Similarly, each sample's prescribed amount of epoxy resin was diluted with ethanol using a magnetic stirrer and a probe-sonicator. After that, the previously prepared graphene-ethanol solution was added with diluted epoxy. The mixer was stirred from 250 to 750 rpm for 2 h and then sonicated for 1 h to make uniform graphene dispersion. Finally, the ethanol was evaporated from the graphene-epoxy mixer by stirring at a low temperature ($\sim 50^\circ\text{C}$). The hardener was added in a stoichiometric 1:10 ratio with the mixture, bringing the final nanocomposite solution to the coating process.

In order to execute the coating, a bed of coating solution was applied to the surface of polished copper foil, the Mayer rod was placed in that

position, and the rod was then pulled in the uncoated direction. At room temperature, uniform pressure and speed were maintained during coating by the rod. Finally, the finished coated surface was kept for 24 h to obtain the interfacial bonding between the coating layer and the copper surface. The chemical compositions of the coating samples are listed in Table 1.

2.5. Characterization of graphene-reinforced epoxy nanocomposite (GREN) coatings

The crystalline information of pristine graphite, synthesized graphene, pure epoxy, and GREN coatings was obtained using a Rigaku Smart Lab X-ray diffractometer equipped with monochromatic CuK α radiation at a wavelength of 1.5418 Å. Test specimens were prepared as powder samples and placed on a slide holder for analysis. With a scan rate of 2° min⁻¹, an accelerating voltage of 40 kV, and a current of 40 mA, the X-ray intensity was observed in the range of 10° ≤ 2θ ≤ 60° at room temperature. The associated peak orientation between specific angular and diffracted intensities enabled the identification of the sample behavior. Mono Vista CRS + Raman spectrometer was used to characterize the graphene. A thin film of graphene on a glass plate was used as a specimen, and the Laser excitation energy was 532 nm for characterization.

A spectrum two Fourier Transform Infrared Spectroscopy (FTIR) spectrometer (Perkin Elmer, USA) was employed for the identification of functional groups of the pristine graphite, synthesized graphene, pure epoxy, and GREN coatings. The spectra were recorded at wavelengths ranging from 500 to 4000 cm⁻¹, with the characteristic peaks designated and fitted depending on the functional groups.

The surface morphology and elemental composition of the pristine graphite and synthesized graphene were examined using a Field Emission Scanning Electron Microscope (FESEM) (JEOL, JSM 7610F) equipped with an Energy Dispersive X-ray Spectrometer (EDX). An accelerating voltage of 15 kV was used for these analyses, with magnifications ranging from 5000X to 50000X and resolutions ranging from 1 μm to 100 nm. A scanning electron microscope (SEM) (Hitachi, SU1510) was used to investigate the surface morphology of the fabricated GREN coatings. An exciting voltage of 20 kV, magnifications ranging from 1000X to 2700X, and resolutions between 50 μm and 20 μm were employed.

2.6. Measurement of multi-physical properties

2.6.1. Coating thickness and surface roughness

The thickness and surface roughness of the nanocomposite coatings were measured by the Kett coating thickness tester (model: LZ-990) and Taylor Hobson surface roughness tester (model: Surtronic S128), respectively. In both cases, a calibrated device was used to perform the test. For each sample, the average value was calculated after collecting data from several locations on the surface.

2.6.2. Adhesion strength

The adhesive strength of the coating to the metal substrate is a key requirement for exhibiting the coating's barrier properties. The cross-cut method was used to evaluate the adhesion property of nanocomposite

coatings. The test was performed according to the ASTM D3359 standard, where the adjacent cutting distance was 1.0 mm with the cutting depth completely penetrated to the metal substrate. According to this standard, coating adhesive strength is divided into six levels (5B-0B), with 5B indicating completely smooth cross-cut patterns, 4B indicating equal or less than 5 % has been affected, 3B meaning greater than 5 % but equal or less than 15 % has been affected, 2B indicating more than 15 % but equal or less than 35 % has been affected, and 1B indicating greater than 35 % but equal or less than 65 % has been affected.

2.6.3. Surface wettability and water absorptivity

The surface wettability of fabricated coatings, indicating the surface affinity to the water, was analyzed using an Optical tensiometer via water contact angle (WCA) measurement. The surface has a high WCA, which indicates its hydrophobic nature. To investigate the WCA between the coating surface and water droplet, about 5 μL of the water drop was placed on the nanocomposite coatings, and the images of interfaces were captured within two seconds by a Digital SLR camera and analyzed by ImageJ software. This test was performed at room temperature, and the WCA was calculated using an average of ten measurements taken on various points on the coated surface.

Water absorption (Q_w) of epoxy and GREN coatings was calculated by using the following equation (Eq. No. 1)

$$Q_w = \frac{w_f - w_i}{w_i} \times 100\% \quad (1)$$

Where, w_i and w_f are the weight of the coatings before and after immersion in demineralized water, respectively. Three parallel samples of each coating were tested to determine the average value. To remove the excess water on the surface of the samples before measurement, they were dried using non-woven cotton. The weight of the coated samples was measured using a microbalance with a precision of 0.00001 g. This test was carried out for a period of 20 days.

2.6.4. Thermal stability

Thermogravimetric analysis (TGA) is one of the most widely used techniques for studying materials' thermal stability and decomposition at various temperatures. This work investigated the thermal stability of GREN coatings using the EXSTAR 6000 TG/DTA 6300 (Seiko, Japan) setup. This experiment was conducted in a nitrogen atmosphere with a heating rate of 20 °C/min.

2.6.5. Electrical conductivity

The direct current (DC) electrical conductivity of GREN coatings was measured using the standard two-probe approach. Silver paint was used to make contact between the probes and the coated surface. The Hioki digital multi-meters DT4281 was used for the measurements. The following equation (Eq. No. 2) is used to calculate sample resistance.

$$R = \Delta V / I \quad (2)$$

Where ΔV is the voltage drop, and I is the current that passes through the sample while neglecting the contact resistance. The electrical conductivity is calculated using the formula $\sigma = \beta/R$, where β is the geometrical parameter. The mean value of electrical conductivity was calculated at room temperature by repeating the measurement five times for each sample.

2.7. Anti-corrosion properties

2.7.1. Immersion study

The corrosion resistance of the GREN coatings was investigated using a 600 h immersion in a 3.5 wt% NaCl solution test. Samples for immersion study were cut to a size of 2.5 cm × 1 cm, sealed on the edges and backside, and cleaned with deionized water. The specimens were then placed at ambient temperature in a 3.5 wt% NaCl solution. Samples were taken for observation with digital photographs, SEM images, and

Table 1

Chemical compositions of GREN coatings.

Samples	Compositions	
	Epoxy (wt.%)	Graphene (wt.%)
S0	100.0	0
S1	99.0	1
S2	98.0	2
S3	97.0	3
S4	95.0	5

changes in electrical conductivity measurement over 600 h after immersion.

2.7.2. Electrochemical analysis

In order to fabricate efficient protective coatings against corrosion, electrochemical analysis (cyclic voltammetry and potentiodynamic polarization) was performed on the GREN-coated Cu surface in 3.5 wt% NaCl solution. The experiment was carried out on a Basi Epsilon electrochemical workstation with a C-3 electrochemical cell. In this test, both the working electrode (GREN-coated Cu) and auxiliary electrode (platinum plate) with a surface area of 1.0 cm^{-2} were submerged in the electrolyte solution, while the Ag/AgCl electrode was used as a reference electrode. Electrochemical measurements were performed in the potential range from 1.0 to 1.0 V with a scan rate of $100 \text{ mV}\cdot\text{s}^{-1}$.

3. Results and discussion

3.1. Characterization of graphene-reinforced epoxy nanocomposite (GREN) coatings

3.1.1. X-ray diffraction, Raman and fourier-transform infrared spectroscopy analysis

The XRD patterns of pristine graphite, synthesized graphene, pure

epoxy, and GREN coatings are shown in Fig. 1a. A strong and sharp carbon (C) peak at $2\theta = 26.6^\circ$ was observed, indicating the natural graphite. This is hexagonal graphite's characteristic peak (002) with a d-spacing of 0.34 nm (Low et al., 2020). The main C peak intensity of graphite was reduced drastically, and it transformed into graphene due to separation from the precursor graphite by the electrochemical exfoliation process (Salverda et al., 2022). Pure epoxy shows a wide peak at $2\theta = 17.9^\circ$ due to the amorphous phase of epoxy (Abdullah and Ansari, 2015). In the XRD pattern of GREN coatings, a broad epoxy peak and a characteristic C peak (002) from graphene were observed, indicating the intercalation dispersion of graphene in the epoxy matrix.

Fig. 1b shows the Raman spectra of the pristine graphite and synthesized graphene. The pristine graphite displays a sharp peak at 1597 cm^{-1} from sp^2 C atoms denoted by G-band, whereas the synthesized graphene shows all three bands at 1363 cm^{-1} (D-band), 1600 cm^{-1} (G-band), and 2661 cm^{-1} (2D-band). However, the position and intensity of all three bands were shifted in synthesized graphene, which might be attributed to the graphene with possible defects during the electrochemical exfoliation process. However, Raman spectra of synthesized graphene show a similar shape of G-band to the pure graphite, where the position and intensity of Raman bands were shifted during the exfoliation process. The specific Raman bands and intensity ratios may reveal important details about the structure of graphene. For example, the I_D/I_G

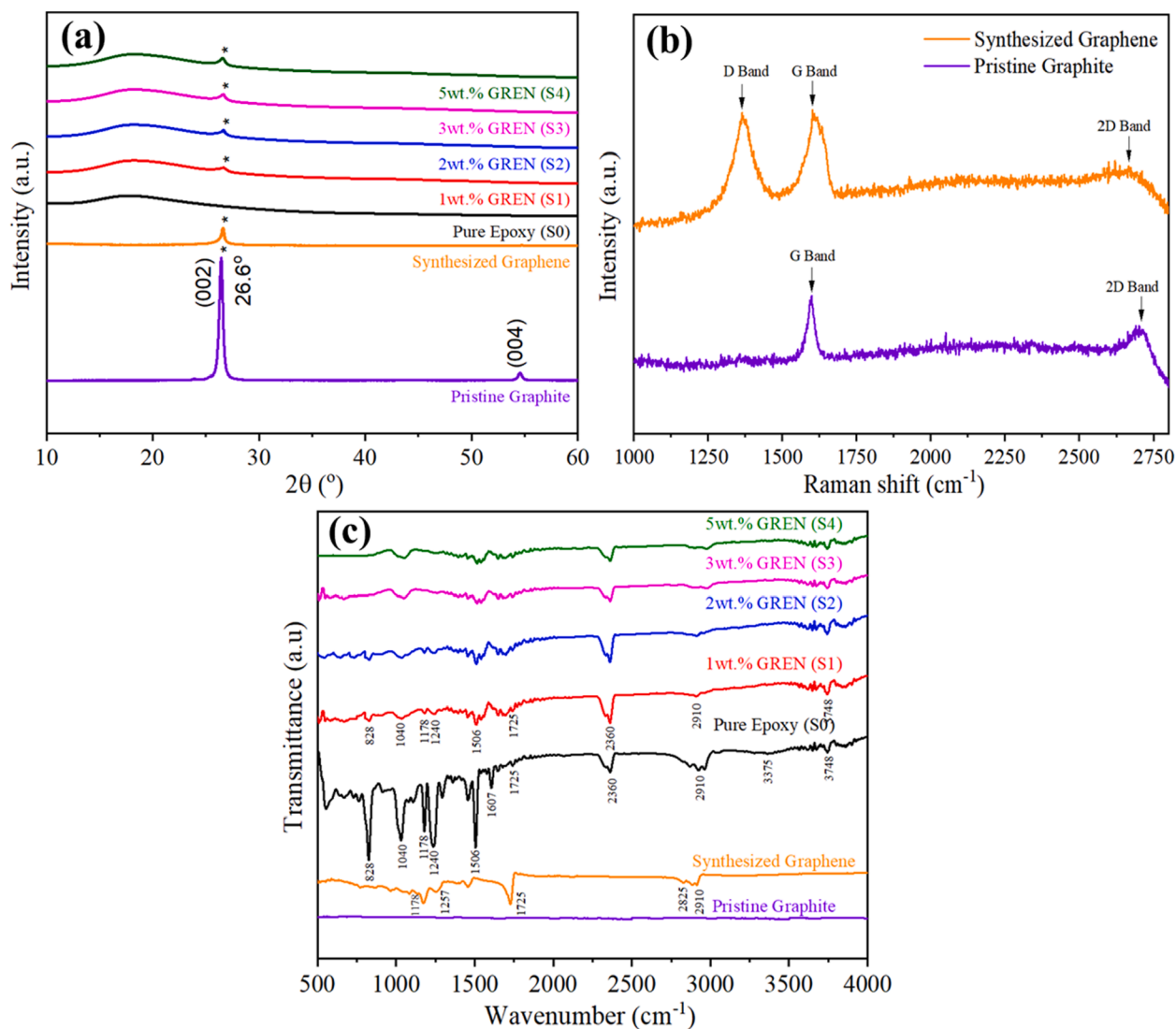


Fig. 1. (a) XRD patterns of pristine graphite, synthesized graphene, pure epoxy, and GREN coatings, (b) Raman spectra of pristine graphite and synthesized graphene, and (c) FTIR spectra of pristine graphite, synthesized graphene, pure epoxy, and GREN coatings.

band intensity ratio represents defects (edges, vacancies, ripples, etc.), while the I_{2D}/I_G band intensity ratio depicts the number of layers in graphene (Shen and Lua, 2013; Khan et al., 2017; Ferrari et al., 2006). The Raman band intensity ratios obtained from graphene are listed in Table 2. The synthesized graphene shows $I_D/I_G = 0.98$ and $I_{2D}/I_G = 0.76$ characteristic ratios, indicating a few defects and multilayered graphene structure, respectively (Geng et al., 2011). The defects might be due to the stacking of graphene layers.

The Fourier-transform infrared (FTIR) study evaluates different bonding states of chemical elements within the pure epoxy and the GREN coatings. Fig. 1c illustrates the FTIR spectra of as-received graphite, synthesized graphene, epoxy, and GREN coatings. The raw graphite spectrum shows a weak stretching vibration at 1678 cm^{-1} , relating to the presence of C = C. The FTIR spectrum of synthesized graphene shows the peaks at 2910 cm^{-1} and 2825 cm^{-1} , representing the C-H group's stretching vibration. The peaks at approximately 1725 cm^{-1} represent carboxyl C = O stretching, at 1257 cm^{-1} and 1178 cm^{-1} represent C-O stretching, while the peak at 966 cm^{-1} is attributed to the C = C bond. The spectra of GREN coatings show a similar peak as pristine graphene at 2910 cm^{-1} , representing the stretching vibration of the C-H group, at approximately 1725 cm^{-1} , representing carboxyl C = O stretching, and at 1178 cm^{-1} represents C-O stretching. The hydroxyl and carboxyl functional groups are shown by the peaks at 3748 cm^{-1} and 1506 cm^{-1} . Peaks around 2360 cm^{-1} can be connected to the C-H (methine) bond vibration of epoxy resin, while major peaks at 1240 cm^{-1} and 1040 cm^{-1} show pure epoxy configuration (amide) (Upadhyay and Kumar, 2019). Similar to this, pure epoxy and GREN coatings show the functional stretching vibrations of N-H bonding at 828 cm^{-1} .

3.1.2. Surface morphology

Fig. 2 shows the FESEM images of the precursor graphite and synthesized graphene and their corresponding EDX spectra and particle size (thickness) of synthesized graphene. In Fig. 2a, as-received graphite revealed a regular plane shape, which is the typical morphology of the graphite surface (Ayati and Ghorbani, 2021). The quantitative analysis from EDX indicated up to 97.57 % carbon and only 2.43 % oxygen in the precursor graphite, which is a good sign for pure graphene extraction. The synthesized thin-layer graphene sheets are observed in Fig. 2b, indicating the features of a high surface/volume ratio due to the organized two-dimensional structure of graphene (Li et al., 2012). The EDX analysis showed up to 83.62 % carbon and 16.38 % oxygen in the graphene. The average particle size of the graphene was 20.61 nm, as shown in Fig. 2c, which was confirmed by measuring more than 100 edges of the graphene sheets.

Fig. 3 shows the SEM images of the surface morphology of prepared pure epoxy coating and GREN coatings containing different graphene contents. In Fig. 3a, the pure epoxy coating contains micro-pores and cavities on its surface, forming during the epoxy's curing period. These micro-pores and cavities are responsible for making easy access to the corrosive environment into the base metal. It is observed that the incorporation of 1–2 wt% graphene in epoxy reduced the micropores on coating surfaces, but the introduction of 3–5 wt% graphene made the surfaces completely flawless due to uniform dispersion, as shown in Fig. 3b–e. It is hypothesized that the graphene formed an interconnecting network through the epoxy resin and confirmed lesser agglomeration when its concentration reaches 3–5 wt% (Abakah et al., 2021). The uniform distribution can be attributed to the better interaction with the epoxy matrix due to the high surface area of graphene. These graphene interconnecting GREN coating layers act as a protective film on copper

Table 2

Characteristic intensity ratio of I_D/I_G and I_{2D}/I_G in synthesized graphene measured from corresponding Raman spectra (average values are reported).

Samples	I_D	I_G	I_{2D}	I_D/I_G	I_{2D}/I_G
Synthesized Graphene	1684	1703	1303	0.98	0.76

surfaces, which is associated with the prevention of corrosion as well as being electrically conductive (Wang et al., 2018).

3.2. Multi-physical properties of nanocomposite coatings

3.2.1. Coating thickness and surface roughness

An optimal coating thickness is crucial for obtaining the desired surface roughness, adhesive strength, and corrosion resistance (Kato et al., 2014). The average coating thickness of all samples was measured as 20 μm , as listed in Table 3. Interestingly, there was no remarkable variation in coating thickness by increasing graphene content in the epoxy matrix. The surface roughness (Ra) of pure epoxy and GREN coatings are measured and reported in Fig. 4 and Table 3. It is observed that the surface roughness of nanocomposite coatings decreased with the increase of graphene wt.% in epoxy resin (Thakur et al., 2019). The average surface roughness of the 3 wt% and 5 wt% GREN coatings were measured as 0.33 μm and 0.25 μm , respectively, which indicates that graphene contents sufficiently cover the epoxy matrix surface area than the 1 wt% (0.72 μm) and 2 wt% (0.64 μm) GREN coatings. The addition of 5 wt% graphene in epoxy resin exhibited 73 % lower surface roughness as compared to the pure epoxy coating (0.93 μm). High surface roughness is associated with cracks, pits, embedded particles, and other coating irregularities. So, the path that the corrosive solution takes to reach the metal's surface can be directly influenced by the roughness of coating surface. The fact that graphene particles filled the micropores, voids, or cavities in the epoxy matrix that the cause of the decreased surface roughness (Bandeira et al., 2017).

3.2.2. Adhesion property

Pure epoxy coating and GREN coatings on copper substrates were tested for adhesion property analysis. Table 4 shows the adhesion property of the coating samples examined by the cross-cut test. In comparison to pure epoxy coating (level 3B), which had a cross-cut pattern detachment rate of more than 5 %, GREN coatings displayed excellent adhesion properties. After the cross-cut test, graphene (2, 3, and 5 wt%) reinforced epoxy coatings maintained their integrity with a clean cutting edge and attained adhesion level 5B. However, the adhesion level of 1 wt% GREN coating was 4B, which indicates that a minimum amount of cross-cut pattern (less than 5 %) was detached. Areas of the cross-cut pattern of the coating samples S0 and S1 detached due to wedge spallation failure brought on by the applied compressive stress along the scratch groove and in front of the moving cutter (Xiong et al., 2019).

GREN coatings adhered well to the copper substrate since the graphene made a strong interaction with the epoxy. Additionally, the incorporation of graphene nanofillers into epoxy made the coating denser blocked the micro-pores and cavities of epoxy, and may suppress the coating cracking when subjected to external force (Rajitha and Mohana, 2020). The strong adhesion property indicates that the graphene-reinforced epoxy coatings may hinder the penetration of a corrosive environment, which is the basis for the potential anti-corrosion behavior of the coatings.

3.2.3. Surface wettability and water absorptivity

The wettability of the coating surfaces can be assessed when the water contact angle (WCA) is calculated. According to the WCA, surfaces are classified as hydrophobic if the contact angle is greater than 90° , hydrophilic if the angle is less than 90° , and super hydrophobic if the contact angle is between 150° and 180° (Khan et al., 2022). Fig. 5 shows the changes in WCA of epoxy coatings with the variation of graphene content. The WCA of S0, S1, S2, S3, and S4 is recorded as 65.78° , 77.53° , 85.72° , 94.28° , and 102.06° , respectively which indicates the hydrophilic nature of the epoxy coating surface becomes hydrophobic with the increase of graphene contents. The increase in contact angle can be attributed to the hydrophobic characteristics of graphene, which influenced the coating tends to reduce water absorption by the surface

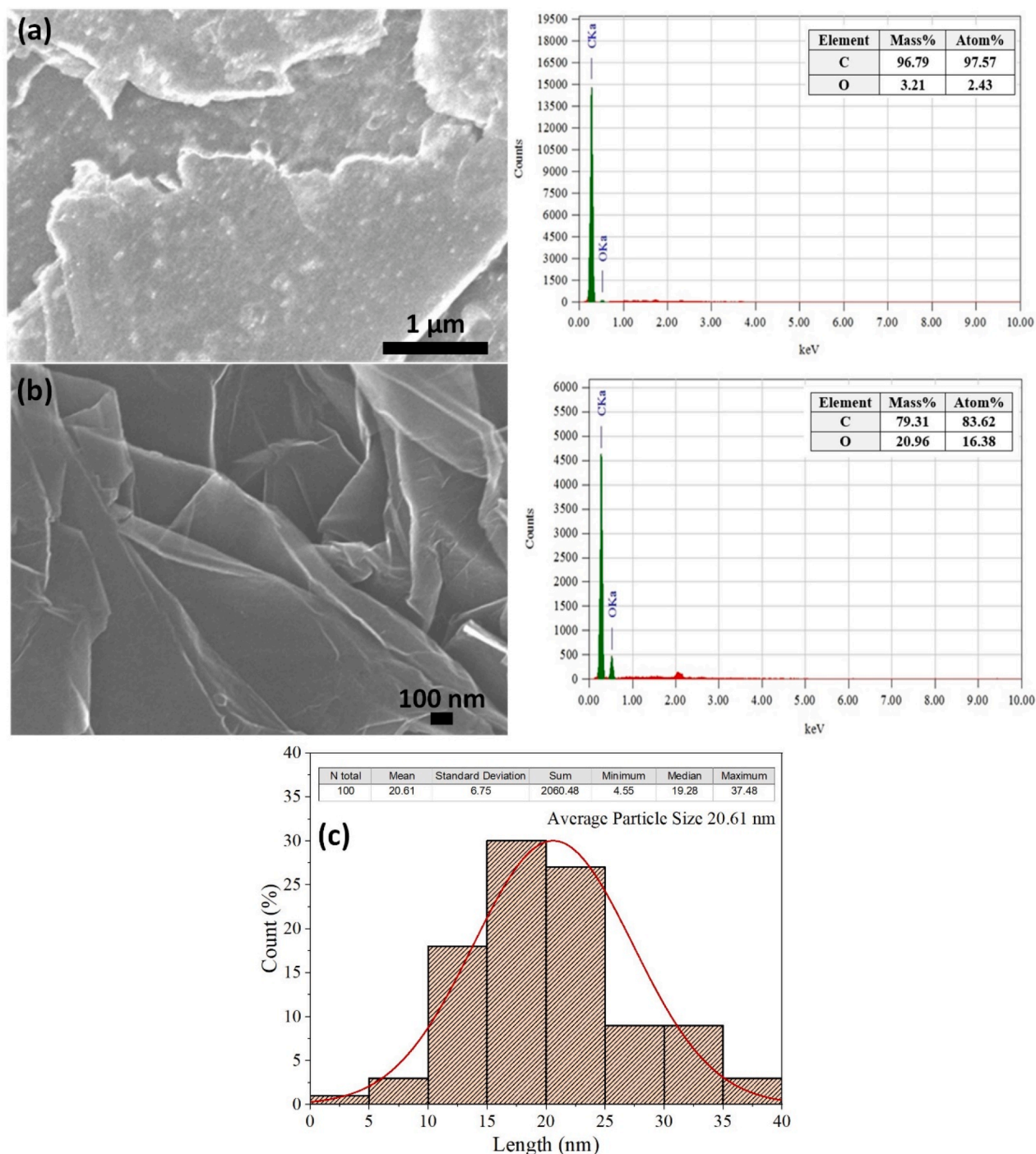


Fig. 2. FESEM image of (a) pristine graphite and (b) synthesized graphene with their corresponding EDX spectra, and (c) particle size of synthesized graphene.

(Darband et al., 2020).

Fig. 6a shows the percentage of water absorption of the GREN coatings after 20 days of immersion. At the initial stage, the curves exhibit a sudden linear growth of water absorption; after that, they rose gradually with the immersion time and finally reached an equilibrium level (Chen et al., 2017). The equilibrium stage indicates the saturation level of water absorption by the coatings, which is one of the leading parameters of the coatings. The saturation level of water absorption by the nanocomposite coatings is summarized in Table 5. It is observed that coatings were not saturated at the same time or to the same degree. The saturation level of water absorption of 5 wt%, 3 wt%, 2 wt%, and 1 wt% of GREN coatings reached approximately 0.81 %, 1.1 %, 1.28 %, and

1.65 % on the 8th, 10th, 12th, and 14th days, respectively. On the 16th day, the pure epoxy coating reached 1.98 % water absorption, ensuring that the graphene incorporation with epoxy declined the water permeability of the nanocomposite coatings by blocking the epoxy's micropores, voids, and cavities (Salom et al., 2018).

3.2.4. Thermogravimetry analysis (TGA)

Thermogravimetry analysis, as shown in Fig. 6b, was used to investigate the thermal stability of nanocomposite coatings. The onset of thermal degradation at 5 % mass loss (T_{on}), thermal degradation at 50 % mass loss ($T_{50\%}$), and mass loss at 500 °C (W_{500}) are displayed in Table 5. It is observed that pure epoxy (S0) has the highest mass loss

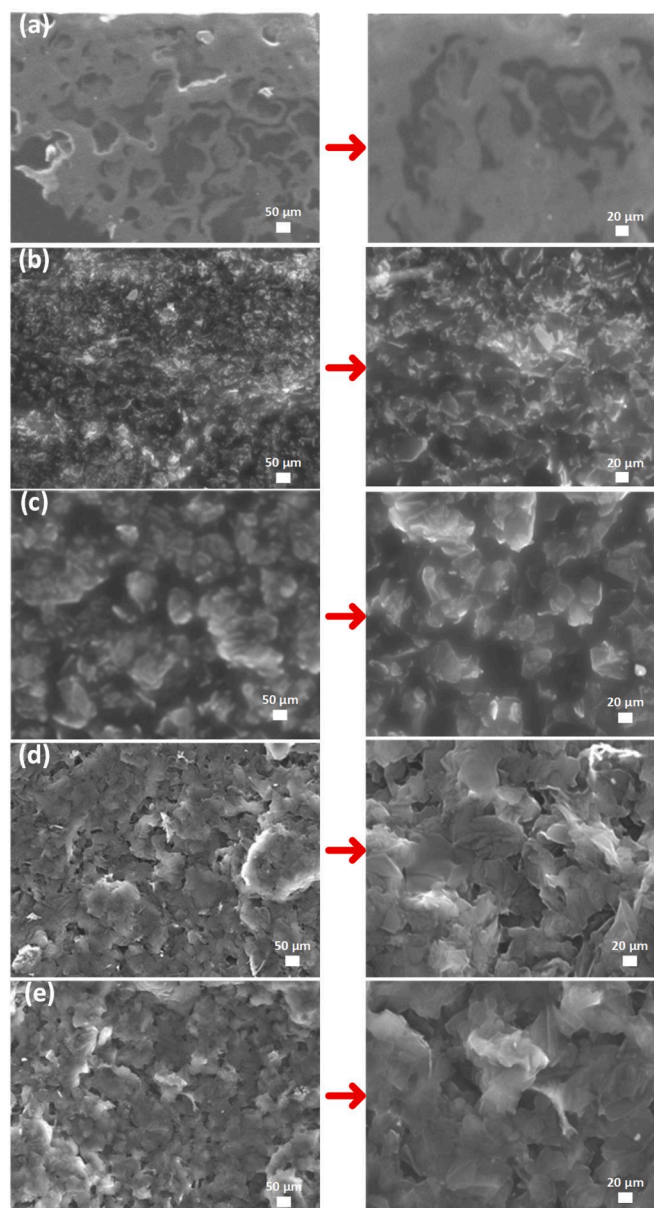


Fig. 3. SEM images of coatings: (a) pure epoxy, (b) 1 wt% GREN, (c) 2 wt% GREN, (d) 3 wt% GREN, and (e) 5 wt% GREN.

Table 3

Coating thickness and surface roughness of pure epoxy and graphene-reinforced epoxy nanocomposite coatings.

Samples	Graphene (wt. %)	Coating Thickness (μm)	Surface Roughness, Ra (μm)
S0	0	22.36 ± 0.65	0.93 ± 0.021
S1	1	17.27 ± 0.58	0.72 ± 0.019
S2	2	18.81 ± 0.51	0.64 ± 0.013
S3	3	21.37 ± 0.67	0.33 ± 0.012
S4	5	17.24 ± 0.52	0.25 ± 0.011

compared to other tested nanocomposite coatings. The significant weight loss in the pure epoxy coating is caused by the softening behavior. As the temperature increases during the test, the intermolecular contact between molecules declines, hence impacting the bonding of polymer chains. Consequently, the intermolecular distance among epoxide molecules expands, leading to a decrease in the overall rigidity and a reduction in the thermal capacity of pure epoxy. Because of this,

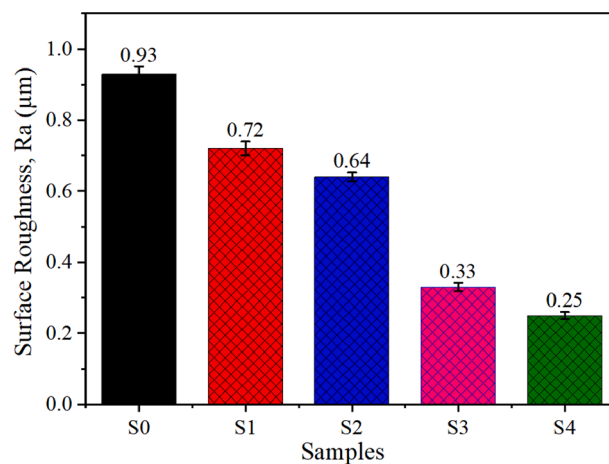


Fig. 4. Surface roughness of pure epoxy and graphene-reinforced epoxy nanocomposite coatings.

pure epoxy exhibits significant weight loss and its capacity to tolerate high temperatures deteriorates. However, the weight loss trend of pure epoxy coating (S0) went suddenly upward from 96.49 °C to 275 °C, which is an abnormal phenomenon that could be the excess mass gain during the TGA test. Some oxygen molecules are absorbed during the sample preparation for the thermogram test, resulting in an increase in sample mass. One more thing that have contributed to the mass gain is the oxidation inside the thermogravimetric cell, which produced extra substances (Upadhyay and Kumar, 2019; Feng et al., 2019).

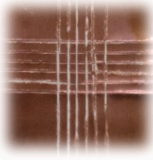
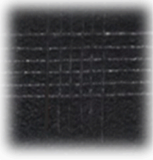
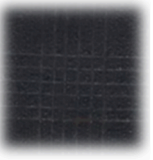
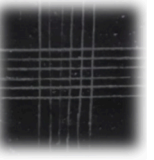
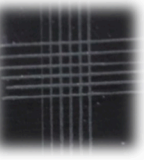
The GREN coatings became more thermally stable as the graphene content increased from 1 to 5 wt%. The onset thermal degradation (T_{on}) for S0 was 313.67 °C, whereas for S1, S2, S3, and S4, the respective values were 234.85 °C, 327.60 °C, 331.72 °C, and 341.65 °C. It was found that GREN coatings are more thermally stable than pure epoxy, except for 1 wt% GREN (S1) at the initial stage. The thermal degradation at 50 % mass loss ($T_{50\%}$) of S0 was 380.44 °C. For S1, S2, S3, and S4, this temperature climbed to approximately 390.07, 406.22, 443.61, and 456.89 °C, respectively. The observed phenomenon can be attributed to the significant interaction between graphene nanofillers and the residual epoxy matrix, resulting in enhanced thermal resistance. At 500 °C, pure epoxy (W_{500}) lost 90.5 % of its mass; for S1, S2, S3, and S4, this dropped to 89.6, 68.89, 53.55, and 52.0 %, respectively. The outstanding thermal stability and a significant reduction in mass loss observed in the GREN coatings can be attributed to several factors. Firstly, the high aspect ratio of graphene, along with its proper dispersion within the coating matrix, contributes to enhanced thermal stability. Additionally, the higher cross-linking density and increased interaction between graphene and epoxy, without agglomeration, result in a more significant hindrance to heat transfer and movement within the polymeric chains. These combined effects contribute to the improved thermal stability of the GREN coatings (Kumar et al., 2019; Gong et al., 2015).

3.2.5. Electrical conductivity

In several areas, such as aerospace, electronic packaging, and mining, epoxy resins as adhesive materials are highly recommended to have electrical conductivity. In the above-mentioned applications, the electrical conductivity of a material of 10^{-6} Scm^{-1} is sufficient as an anti-static material (Mokhtari et al., 2021). Graphene has demonstrated its ability to create electrically conductive polymers even though they are nonconductive in their natural state (Wang et al., 2021). Fig. 6c depicts the improvements in electrical conductivity of epoxy nanocomposite coatings with graphene inclusion. The electrical conductivity of pure epoxy coating is reported as $10^{-14} \text{ Scm}^{-1}$, which is similar to the previous report (Rashid et al., 2022). Addition of only 1.0 wt% graphene in

Table 4

The adhesive strength of pure epoxy and graphene-reinforced epoxy nanocomposite coatings.

Samples	S0	S1	S2	S3	S4
Cross-cut pattern					
Adhesion level	3B	4B	5B	5B	5B

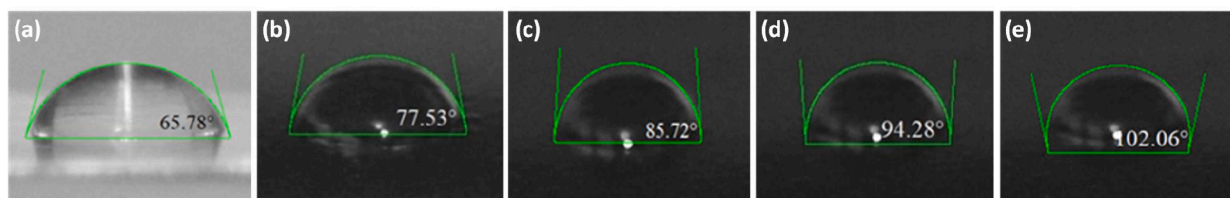


Fig. 5. Water contact angle of coatings: (a) pure epoxy, (b) 1 wt% GREN, (c) 2 wt% GREN, (d) 3 wt% GREN, and (e) 5 wt% GREN.

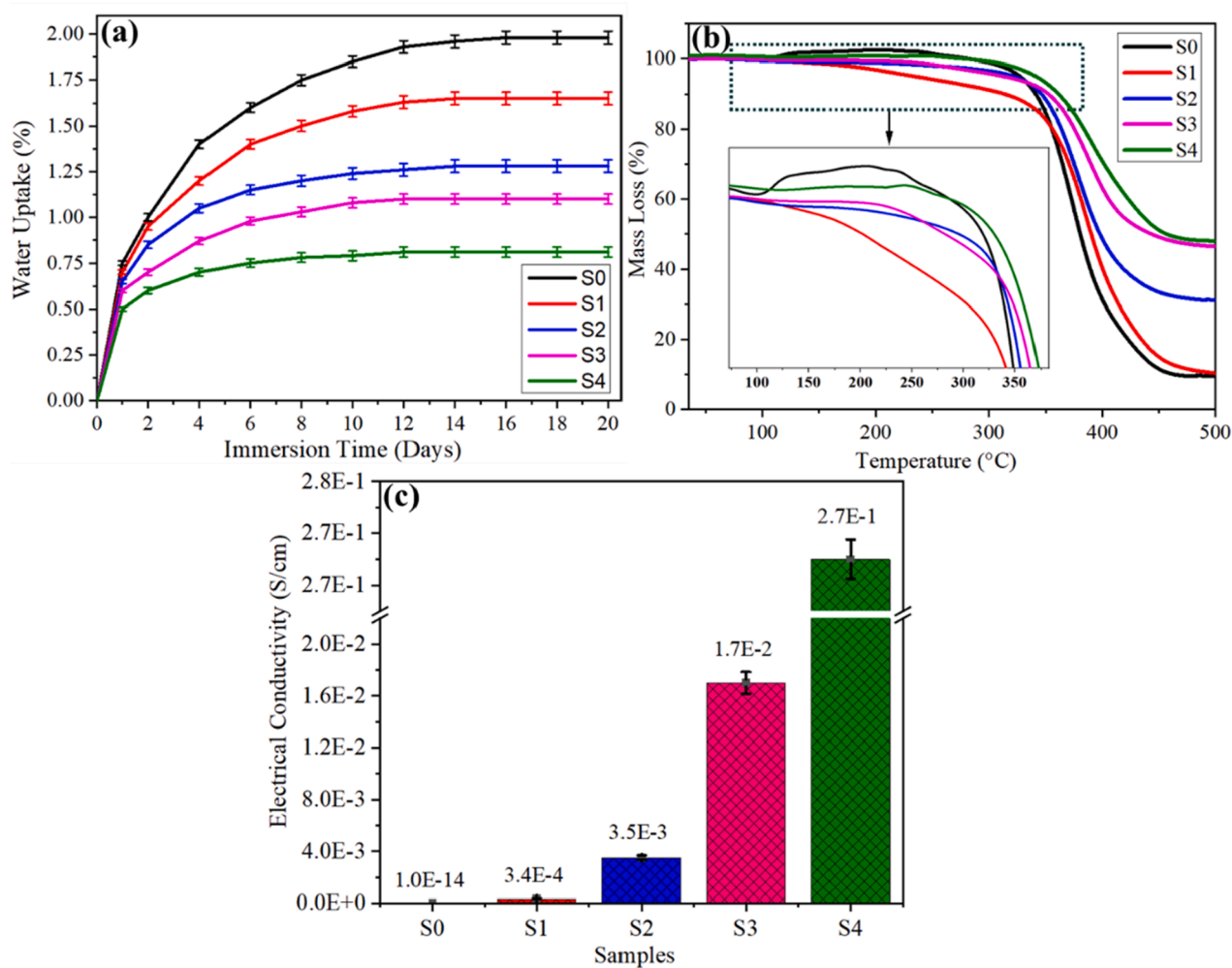


Fig. 6. (a) Percentage of water uptake (absorption), (b) thermogravimetry analysis, and (c) electrical conductivity of pure epoxy and graphene-reinforced epoxy nanocomposite coatings.

Table 5

Maximum absorbed water content, thermal degradation, mass loss, and electrical conductivity of pure epoxy and graphene-reinforced epoxy nanocomposite coatings.

Samples	Maximum absorbed water content (%)	The onset of thermal degradation at 5 % mass loss (T_{on}) (°C)	Thermal degradation at 50 % mass loss ($T_{50\%}$) (°C)	Mass loss at 500 °C (W_{500}) (%)	Electrical conductivity (Scm^{-1})
S0	1.98	313.67	380.44	90.50	10^{-14}
S1	1.65	234.85	390.07	89.60	3.4×10^{-4}
S2	1.28	327.60	406.22	68.89	3.5×10^{-3}
S3	1.10	331.72	443.61	53.55	1.7×10^{-2}
S4	0.81	341.65	456.89	52.00	2.7×10^{-1}

epoxy, the electrical conductivity rose to $3.4 \times 10^{-4} Scm^{-1}$ by 10 orders of magnitude, which is in the range of anti-static material. Similarly, 2 wt%, 3 wt%, and 5 wt% of graphene in epoxy showed a steadily increasing trend of electrical conductivity as $3.5 \times 10^{-3} Scm^{-1}$, $1.7 \times 10^{-2} Scm^{-1}$, and $2.7 \times 10^{-1} Scm^{-1}$, respectively. The increasing trend of electrical conductivity with the graphene content indicates that an electrically conductive in-plane pathway might be created by the shear stress-induced bar coating process (Kim et al., 2019). However, the maximum electrical conductivity of 5 wt% GREN coating is far lower than that of pure Cu (generally $10^5 Scm^{-1}$), indicating that graphene is not attached to Cu foil but is orientated inside the epoxy matrix, preventing the corrosion reaction from being accelerated.

3.3. Anti-corrosion properties analysis

3.3.1. Immersion test in 3.5 wt% NaCl solution

Uncoated Cu, pure epoxy, and GREN-coated Cu samples were exposed to 3.5 wt% NaCl solution for 600 h. The digital and SEM images of immersed samples at different immersion times are shown in Fig. 7 and Fig. 8. The bare Cu surface was destroyed catastrophically with the increase of immersion time due to a large number of corrosion products (patinas induced by Cl^-) enclosed after immersion in 3.5 wt% NaCl solution. Since the pure epoxy coating contains micropores, voids, and cavities on its surface, corrosive NaCl solution easily penetrates the base metal and corrodes it with the immersion time.

The addition of graphene in epoxy blocks these micro-pores and cavities of pure epoxy coating. However, the addition of low content (1–2 wt%) of graphene is unable to block a few of the micropores, resulting in insufficient corrosion resistance of the nanocomposite coatings. The diffusion pathways of corrosive media in epoxy coatings prevent effectively with 3–5 wt% of graphene. In SEM morphology (Fig. 8), it is observed that there is no change in the 5 wt% GREN coating surfaces after the immersion in 3.5 wt% NaCl solution for 600 h. It might be attributed to the high density of graphene nanofillers hindering the diffusion of the corrosive agent through the nanocomposite coating.

In Fig. 9, the uncoated Cu and pure epoxy-coated Cu showed a lot of electrical conductivity losses (approximately 98 % and 86 %, respectively) after immersion in 3.5 % NaCl solution for 600 h. In contrast, the GREN-coated Cu samples indicated a slight loss of conductivity in the same environment. 5 wt% GREN coating lost only 13 % of the electrical conductivity after immersion in 3.5 % NaCl solution for 600 h. Since it withstood a corrosive media without losses of electrical conductivity, it is an excellent sign of anticorrosive properties (Kim et al., 2019). Therefore, it is evident that 5 wt% GREN coating exhibits electrically conductive and anticorrosive properties simultaneously.

3.3.2. Electrochemical analysis

The study of cyclic voltammetry (CV) and potentiodynamic polarization (PDP) for the coatings was carried out under the application of 3.5 wt% NaCl solution to understand the electrochemical behavior of these coatings. A comparative cyclic voltammogram of uncoated Cu and pure epoxy-coated Cu is shown in Fig. 10a. Uncoated Cu exhibits two prominent anodic peaks designated as (x) and (y) at 0.2 V and 0.37 V, which relates to the formation of $CuCl^-$ and $CuCl_2^-$ due to the high concentration of Cl^- ions according to reactions (3) & (4) (Kear et al.,

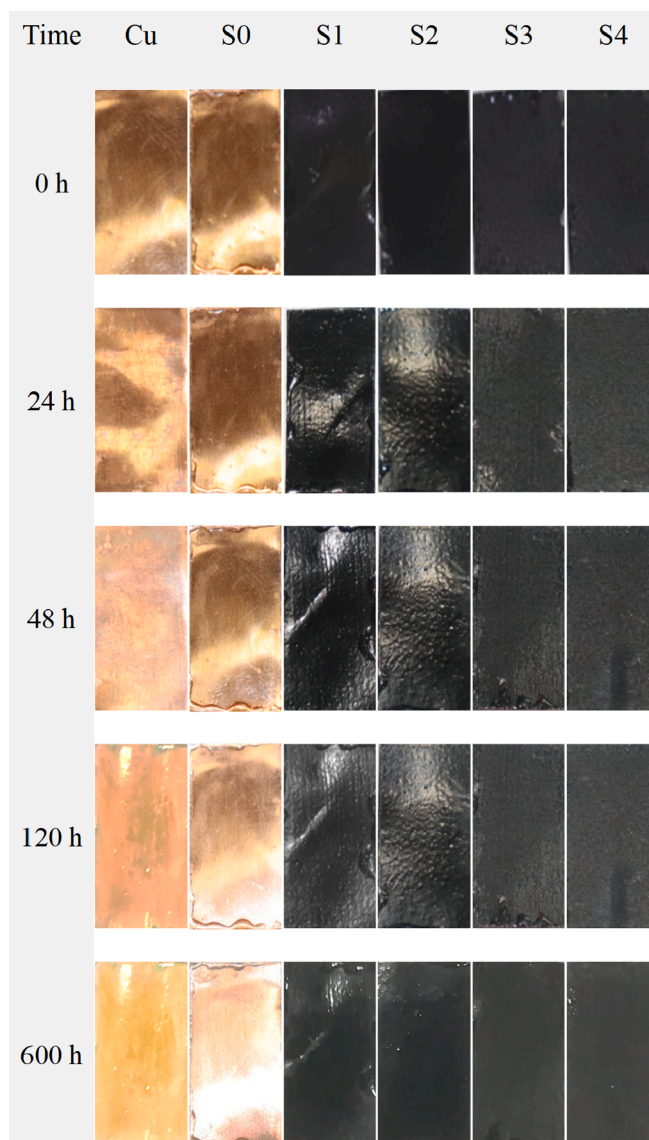


Fig. 7. Digital images of uncoated Cu, pure epoxy, and GREN-coated Cu samples at different immersion times in 3.5 wt% NaCl solution.

2004).



$CuCl_2^-$ can undergo hydrolysis due to the presence of oxygen in the solution according to the reaction (5).



In the case of a cathodic reaction, a reduction peak (z) at $-0.5 V$ may

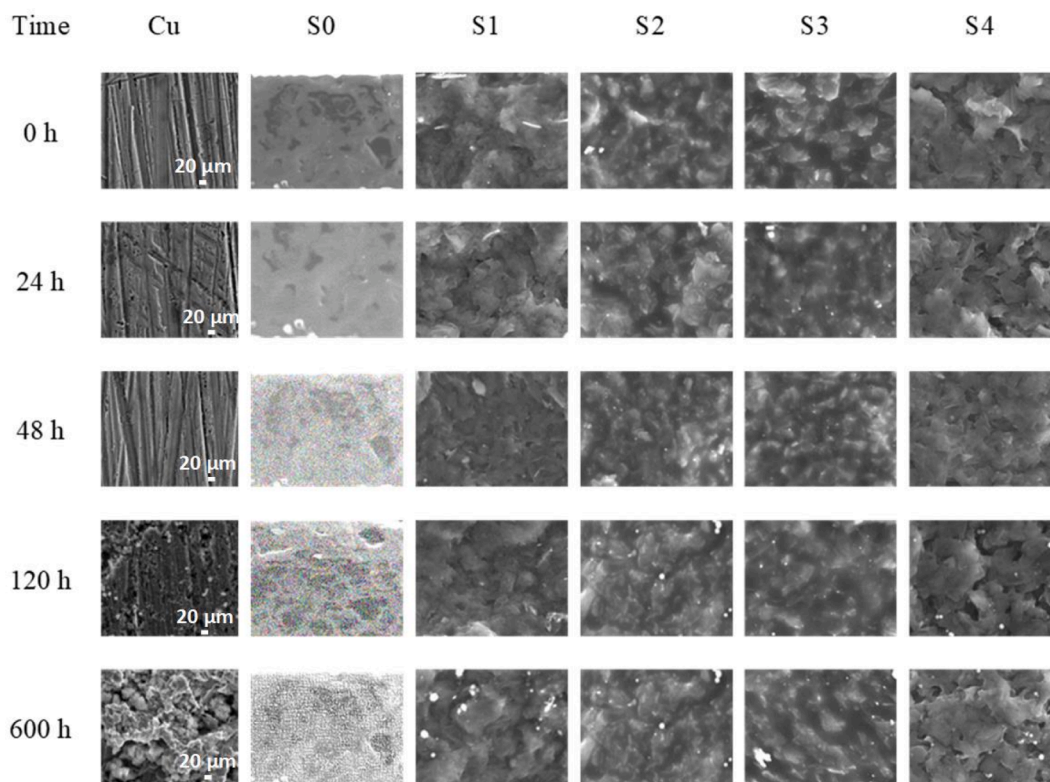


Fig. 8. SEM images of uncoated Cu, pure epoxy, and GREN-coated Cu samples at different immersion times in 3.5 wt% NaCl solution.

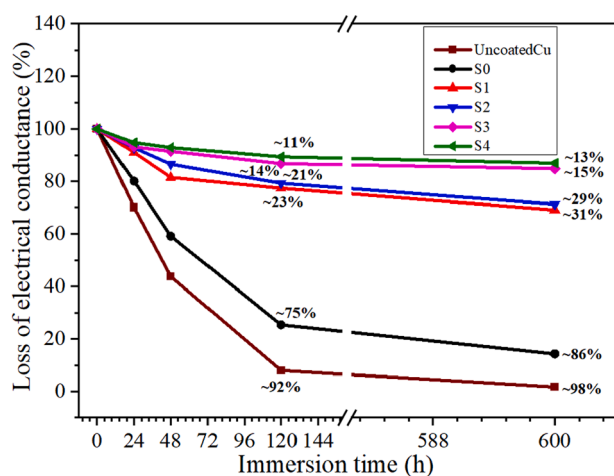


Fig. 9. Electrical conductivity of uncoated Cu, pure epoxy, and GREN-coated Cu samples at different immersion times in 3.5 wt% NaCl solution.

correspond to the reduction of CuCl^- to Cu metal (Karthik and Sethuraman, 2015). It can be seen that the current density of the oxidation–reduction reaction of pure epoxy coating is negligible as compared with the uncoated Cu. However, the pure epoxy coating exhibits the highest current density in comparison with all the GREN coatings, as shown in Fig. 10b. Even in chloride solution, all coated samples had considerably lower current densities of oxidation–reduction processes, indicating diminished electrochemical activity at the coated electrode surfaces (Kim et al., 2019). The highest electrochemical activity of pure epoxy coating is because of the micropores and cavities on its surface that easily penetrate the electrolyte solution to the substrate. The presence of graphene in epoxy effectively blocks the micropores of the coating surface, which causes the current

density of the electrochemical reaction to be significantly reduced in comparison with pure epoxy coating. However, the electrochemical reaction of GREN coatings is noticeably decreased with the increase of graphene contents and therefore the current density of 5 wt% GREN is the lowest among all the GREN coatings.

The potentiodynamic polarization (PDP) curves of uncoated Cu, pure epoxy coating, and GREN coatings are displayed in Fig. 10c. PDP curves are frequently used to quantify the anti-corrosion capability of coatings. Coatings with lower corrosive current and higher corrosive potential generally demonstrated improved anti-corrosion capabilities (Ibrahim et al., 2020). From Fig. 10c, the uncoated Cu showed the highest corrosive current and the lowest corrosive potential, which indicates it corroded faster in 3.5 wt% NaCl solution. However, all the GREN-coated Cu samples exhibited better anticorrosive properties than uncoated Cu and pure epoxy-coated Cu. An increase in the amount of graphene added improved the anti-corrosion property of the GREN coatings. Among all these specimens, 5 wt% GREN coating displayed the highest corrosive potential and the lowest corrosive current.

The changes in corrosion current (I_{corr}) and corrosion rate (CR) of the GREN coatings are obtained by the extrapolation of the PDP curves as shown in Fig. 10d. Uncoated Cu showed a corrosion rate of 3.4×10^{-2} mm per year (mppy), whereas pure epoxy coated Cu exhibited 1.4×10^{-2} mppy CR. Similarly, the addition of graphene in the pure epoxy also showed a decreasing trend in the corrosion rate. The corrosion rate decreased dramatically from 1.4×10^{-2} to 5.0×10^{-5} mppy by increasing graphene content in the epoxy. This outcome is the consequence of graphene filling the micropores and microcracks of the epoxy, which effectively inhibits the diffusion of corrosive fluids.

3.3.3. Anti-corrosion mechanisms of the graphene-reinforced epoxy nanocomposite coatings

Considering the aforementioned findings and analysis, the anti-corrosion mechanisms of pure epoxy and GREN coatings were presented in Fig. 11. The corrosion barrier efficacy of epoxy coating was reduced by the cracks and micro-pores, which were created by

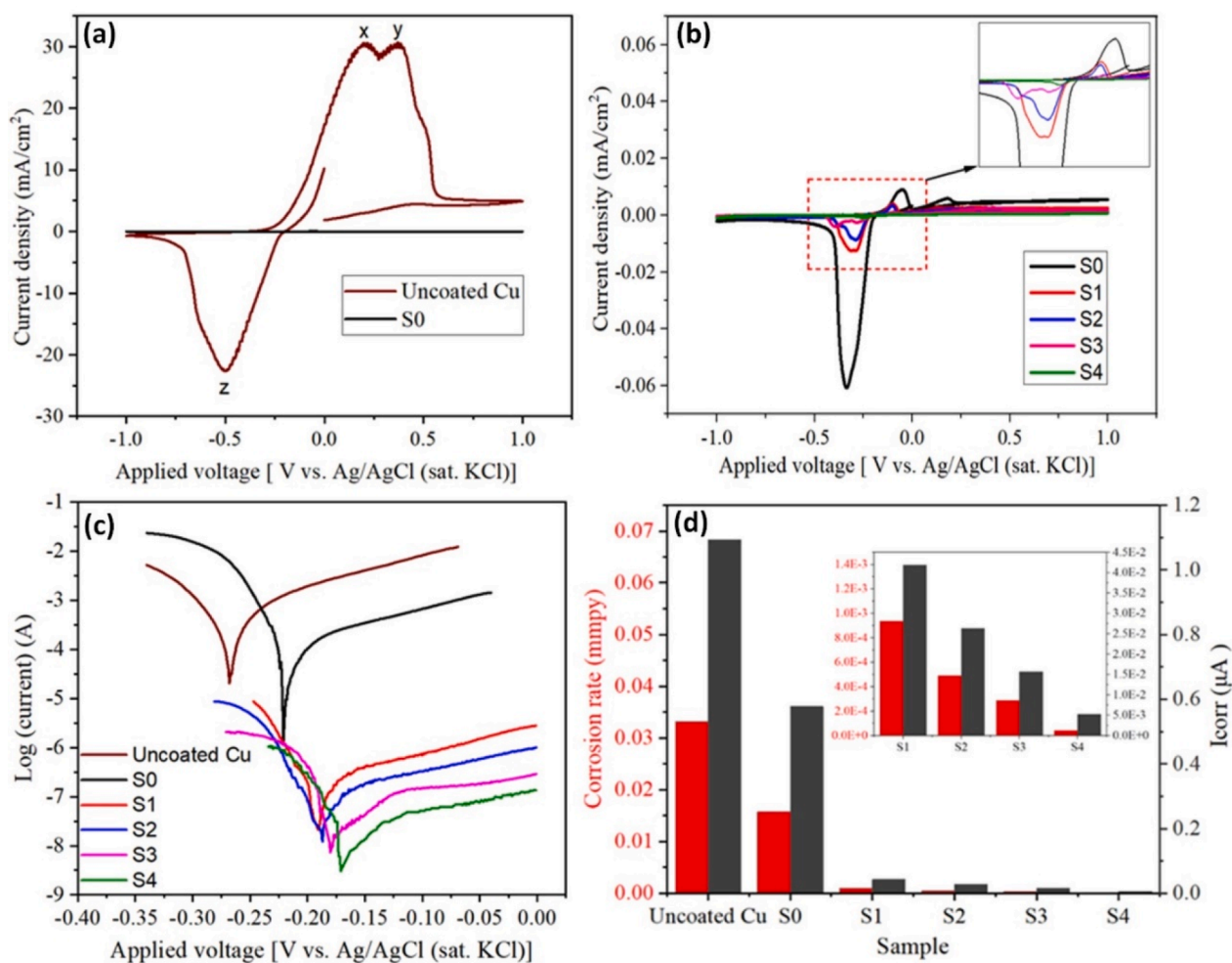


Fig. 10. (a) Cyclic voltammetry of uncoated Cu and pure epoxy coating, (b) cyclic voltammetry of pure epoxy coating and GREN coatings, (c) potentiodynamic polarization curves, and (d) corrosion current (I_{corr}) and corrosion rate (mmpy) for uncoated Cu, pure epoxy coating and GREN coatings.

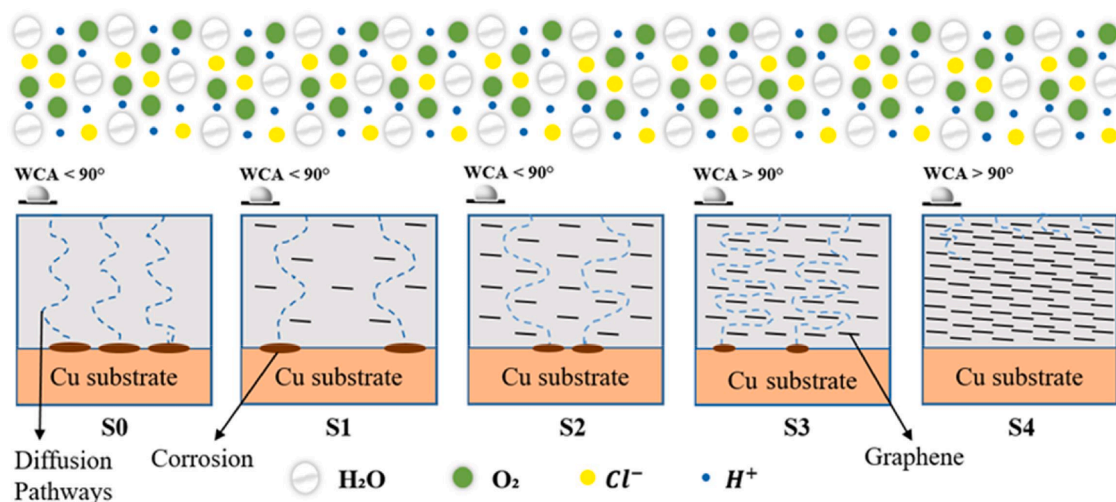


Fig. 11. Anti-corrosion mechanism of epoxy and GREN coatings in 3.5 wt% NaCl solution.

evaporation of the solvent during the production process and acted as pathways for corrosive solution (Cl^- , O_2 , H^+ and H_2O). Due to the inadequate barrier capacity of pure epoxy coating, the corrosive medium quickly penetrated the protective layer interface and damaged the metal substrate. The GREN coatings, on the other hand, demonstrated

improved corrosion protection, which can be attributable to a number of distinct aspects: (i) the interaction of graphene with epoxy contributes to minimizing coating surface defects, (ii) due to the high surface energy of graphene nanofillers, a very hydrophobic nanocomposite coating surface is developed, (iii) at the coating-metal contact, graphene enhances

adhesive strength, and (iv) the impermeable characteristic of graphene creates an efficient surface barrier to the aggressive environment (Cl^- , O_2 , H^+ , and H_2O). The schematic further demonstrates the significance of the graphene wt.%, indicating that a higher graphene wt.% results in stronger barrier properties and a more tortuous diffusion path for a corrosive medium. However, among all the GREN coatings, 5 wt% GREN displayed the most effective and advanced surface barrier performance that can be used in corrosion-resistant fields.

4. Conclusions

Graphene-reinforced epoxy nanocomposite (GREN) coatings containing 1 wt%, 2 wt%, 3 wt%, and 5 wt% of graphene were fabricated on the copper substrate using a bar coating approach. Their multi-physical properties were demonstrated extensively, including coating thickness, surface roughness, adhesiveness, surface wettability, water absorptivity, electrical conductivity and thermal stability, and anti-corrosion properties. The significant findings of this study are listed as follows:

1. The average coating thickness of each sample was measured as 20 μm . The addition of 5 wt% graphene in epoxy exhibited 73 % lower surface roughness (0.25 μm) as compared to the pure epoxy coating (0.93 μm), the edges of the cross-cut pattern were utterly smooth, indicating 5B adhesion level (none of the squares of the lattice was detached), the surface of the coating became hydrophobic in nature with WCA is 102.06°, and only 0.81 % water absorptivity after an immersion period of 8 days.
2. The electrical conductivity of pure epoxy coating was only $10^{-14} \text{ Scm}^{-1}$, which is in the range of insulative materials. However, 5 wt% GREN coating showed several orders of magnitude increments up to values of around $2.7 \times 10^{-1} \text{ Scm}^{-1}$, which is in the range of conductive polymers.
3. The GREN coatings became more thermally stable as the graphene content increased from 1 to 5 wt%. The onset thermal degradation (T_{on}) of GREN coatings increased from 313.67 to 341.65 °C, degradation temperature at 50 % mass loss ($T_{50\%}$) increased from 380.44 to 456.89 °C, and the mass loss at 500 °C (W_{500}) decreased from 90.5 % to 52.0 % with the addition of 5 wt% graphene in epoxy.
4. In the immersion test in 3.5 wt% NaCl solution for 600 h, GREN coating with 5 wt% graphene prevents the diffusion pathways for corrosive medium and withstood along with a minor loss of electrical conductivity that simultaneously exhibits the electrical conductivity and anticorrosive properties of the coating surface.
5. Cyclic voltammetry (CV) and potentiodynamic polarization (PDP) analysis revealed that the electrochemical reaction of GREN coatings is considerably reduced with the increase of graphene contents, and following the addition of 5 wt% graphene, the corrosion rate fell sharply from 3.4×10^{-2} to 5.0×10^{-5} mmpy.

Due to superior hydrophobicity, thermal stability, electrical conductivity, and corrosion resistance, the GREN coatings can be considered as a multi-functional coating in industrial applications.

Declaration of competing interest

The authors declare that they have no known competing financial interests or personal relationships that could have appeared to influence the work reported in this paper.

Acknowledgment

The authors acknowledge the financial support for this research by the Department of Mechanical Engineering, Dhaka University of Engineering & Technology, Gazipur, Bangladesh. The authors also acknowledge the scientific and technical assistance of the Pilot Plant and Process Development Centre, Bangladesh Council of Scientific and

Industrial Research. In addition, the authors are grateful to the Materials Science Division, Bangladesh Atomic Energy Commission and Wazed Miah Science Research Center, Jahangirnagar University, for providing their testing facilities.

References

- Abakah, R.R., et al., 2021. Comparative study of corrosion properties of different graphene nanoplate/epoxy composite coatings for enhanced surface barrier protection. *Coatings* 11 (3), 285.
- Abdullah, S.I., Ansari, M., 2015. Mechanical properties of graphene oxide (GO)/epoxy composites. *Hbr J.* 11 (2), 151–156.
- Al-Moubaraki, A.H., Obot, I., 2021. Top of the line corrosion: causes, mechanisms, and mitigation using corrosion inhibitors. *Arab. J. Chem.* 14 (5), 103116.
- Ayati, B., Ghorbani, Z., 2021. Enhancement of the electro-activated persulfate process in dye removal using graphene oxide nanoparticle. *Water Sci. Technol.* 83 (9), 2169–2182.
- Bahgat Radwan, A., et al., 2021. Electrospun highly corrosion-resistant polystyrene–nickel oxide superhydrophobic nanocomposite coating. *J. Appl. Electrochem.* 51 (11), 1605–1618.
- Bandeira, R.M., et al., 2017. Influence of the thickness and roughness of polyaniline coatings on corrosion protection of AA7075 aluminum alloy. *Electrochim. Acta* 240, 215–224.
- Bao, Y., et al., 2020. Effect of the feeding mode of cross-linker and microcapsule on the corrosion resistance and hydrophobicity of composite coatings. *Arab. J. Chem.* 13 (12), 9068–9080.
- Chen, C., et al., 2017. Achieving high performance corrosion and wear resistant epoxy coatings via incorporation of noncovalent functionalized graphene. *Carbon* 114, 356–366.
- Chowdhury, M.A., et al., 2022. Advances in coatings on Mg alloys and their anti-microbial activity for implant applications. *Arab. J. Chem.* 15 (11), 104214.
- Dagdag, O., et al., 2020. Fabrication of polymer based epoxy resin as effective anti-corrosive coating for steel: Computational modeling reinforced experimental studies. *Surf. Interfaces* 18, 100454.
- Darband, G.B., et al., 2020. Science and engineering of superhydrophobic surfaces: review of corrosion resistance, chemical and mechanical stability. *Arab. J. Chem.* 13 (1), 1763–1802.
- Fadl, A., et al., 2021. Multi-functional epoxy composite coating incorporating mixed Cu (II) and Zr (IV) complexes of metformin and 2, 2'-bipyridine as intensive network cross-linkers exhibiting anti-corrosion, self-healing and chemical-resistance performances for steel petroleum platforms. *Arab. J. Chem.* 14 (10), 103367.
- Feng, C., et al., 2019. Performance of coating based on β -CD-g-GO/epoxy composites for the corrosion protection of steel. *Int. J. Electrochem. Sci.* 14 (2), 1855–1868.
- Ferrari, A.C., et al., 2006. Raman spectrum of graphene and graphene layers. *Phys. Rev. Lett.* 97 (18), 187401.
- Geng, D., et al., 2011. Nitrogen doping effects on the structure of graphene. *Appl. Surf. Sci.* 257 (21), 9193–9198.
- Gong, L.-X., et al., 2015. Balanced electrical, thermal and mechanical properties of epoxy composites filled with chemically reduced graphene oxide and rubber nanoparticles. *Compos. Sci. Technol.* 121, 104–114.
- Habib, S., et al., 2021. Improved self-healing performance of polymeric nanocomposites reinforced with talc nanoparticles (TNPs) and urea-formaldehyde microcapsules (UFMCs). *Arab. J. Chem.* 14 (2), 102926.
- Haghdadeh, P., et al., 2018. The role of functionalized graphene oxide on the mechanical and anti-corrosion properties of polyurethane coating. *J. Taiwan Inst. Chem. Eng.* 86, 199–212.
- Ibrahim, N.F., et al., 2020. Corrosion inhibition properties of epoxy-zinc oxide nanocomposite coating on stainless steel 316L. *Solid State Phenom.* 307, 285–290.
- Jaseela, P., et al., 2020. Excellent protection of mild steel in sodium chloride solution for a substantial period of time using a hybrid nanocoating of poly vinyl alcohol and Titania. *Arab. J. Chem.* 13 (8), 6921–6930.
- Jena, G., Philip, J., 2022. A review on recent advances in graphene oxide-based composite coatings for anticorrosion applications. *Prog. Org. Coat.* 173, 107208.
- Jouyandeh, M., et al., 2019. Cure kinetics of epoxy/graphene oxide (GO) nanocomposites: Effect of starch functionalization of GO nanosheets. *Prog. Org. Coat.* 136, 105217.
- Jouyandeh, M., et al., 2019. 'Cure Index' for thermoset composites. *Prog. Org. Coat.* 127, 429–434.
- Karthik, N., Sethuraman, M.G., 2015. Assessment of the corrosion protection ability of cysteamine and hybrid sol–gel twin layers on copper in 1% NaCl. *RSC Adv.* 5 (12), 8693–8705.
- Kato, M., et al., 2014. Effects of coating thickness and interfacial roughness on cracking and delamination strength of WC-Co coating measured by ring compression test. *IOP Conference Series: Materials Science and Engineering*. IOP Publishing.
- Kear, G., et al., 2004. Electrochemical corrosion behaviour of 90–10 Cu–Ni alloy in chloride-based electrolytes. *J. Appl. Electrochem.* 34, 659–669.
- Khan, Q.A., et al., 2017. Characterization of reduced graphene oxide produced through a modified Hoffman method. *Cogent Chem.* 3 (1), 1298980.
- Khan, M.Z., et al., 2022. Recent advances in superhydrophobic surfaces for practical applications: A review. *Eur. Polym. J.*, 111481.
- Kim, H., et al., 2019. Electrically conductive and anti-corrosive coating on copper foil assisted by polymer-nanocomposites embedded with graphene. *Appl. Surf. Sci.* 476, 123–127.

- Kumar, R., Mohanty, S., Nayak, S.K., 2019. Study on epoxy resin-based thermal adhesive filled with hybrid expanded graphite and graphene nanoplatelet. *SN Appl. Sci.* 1, 1–13.
- Kwak, J., et al., 2017. Oxidation behavior of graphene-coated copper at intrinsic graphene defects of different origins. *Nat. Commun.* 8 (1), 1549.
- Li, X.-R., et al., 2012. Potassium-doped graphene for simultaneous determination of nitrite and sulfite in polluted water. *Electrochem. Commun.* 20, 109–112.
- Li, K., et al., 2023. Self-healing and wear resistance stable superhydrophobic composite coating with electrothermal and photothermal effects for anti-icing. *Prog. Org. Coat.* 177, 107415.
- Low, I.-M., Albetran, H.M., Degiorgio, M., 2020. Structural characterization of commercial graphite and graphene materials. *J. Nanotechnol. Nanomater.* 1 (1), 23–30.
- Mokhtari, M., et al., 2021. High-performance and cost-effective melt blended poly (ether ether ketone)/expanded graphite composites for mass production of antistatic materials. *Polym. Int.* 70 (8), 1137–1145.
- Nahlé, A., et al., 2022. Experimental and theoretical approach for novel imidazolium ionic liquids as Smart Corrosion inhibitors for mild steel in 1.0 M hydrochloric acid. *Arab. J. Chem.* 15 (8), 103967.
- Nonahal, M., et al., 2018. Epoxy/PAMAM dendrimer-modified graphene oxide nanocomposite coatings: Nonisothermal cure kinetics study. *Prog. Org. Coat.* 114, 233–243.
- Nonahal, M., et al., 2018. Design, preparation, and characterization of fast cure epoxy/amine-functionalized graphene oxide nanocomposites. *Polym. Compos.* 39 (S4), E2016–E2027.
- Pourhashem, S., et al., 2020. Polymer/Inorganic nanocomposite coatings with superior corrosion protection performance: A review. *J. Ind. Eng. Chem.* 88, 29–57.
- Pradhan, S.P., et al., 2022. Conducting polymer composites for antistatic application in aerospace. *Aerosp. Polym. Mater.* 155–187.
- Rajitha, K., Mohana, K.N.S., 2020. Synthesis of graphene oxide-based nanofillers and their influence on the anticorrosion performance of epoxy coating in saline medium. *Diam. Relat. Mater.* 108, 107974.
- Rashid, I.A., et al., 2022. Electrically conductive epoxy/polyaniline composite fabrication and characterization for electronic applications. *J. Reinf. Plast. Compos.* 41 (1–2), 34–45.
- Salom, C., et al., 2018. Mechanical properties and adhesive behavior of epoxy-graphene nanocomposites. *Int. J. Adhes. Adhes.* 84, 119–125.
- Salverda, M., et al., 2022. Electrochemical exfoliation of graphite to graphene-based nanomaterials. *Molecules* 27 (24), 8643.
- Shen, Y., Lua, A.C., 2013. A facile method for the large-scale continuous synthesis of graphene sheets using a novel catalyst. *Sci. Rep.* 3 (1), 3037.
- Shi, Y., et al., 2023. Achieving dual functional corrosion resistance for epoxy coatings under alternating hydrostatic pressure via constructing P-phenylenediamine/Ti3C2Tx hybrids. *Carbon* 201, 1048–1060.
- Song, S., et al., 2021. Multilayer structural epoxy composite coating towards long-term corrosion/wear protection. *Carbon* 183, 42–52.
- Thakur, R., Singh, K., Sharma, D., 2019. Modeling and optimization of surface roughness in end milling of graphene/epoxy nanocomposite. *Mater. Today: Proc.* 19, 302–306.
- Upadhyay, R.K., Kumar, A., 2019. Effect of particle weight concentration on the lubrication properties of graphene based epoxy composites. *Colloid Interface Sci. Commun.* 33, 100206.
- Uvida, M.C., et al., 2022. Nanostructured poly (methyl Methacrylate)–Silica coatings for corrosion protection of reinforcing steel. *ACS Appl. Nano Mater.* 5 (2), 2603–2615.
- Verma, A., et al., 2023. Engineering defect concentration and morphology of green graphene for the development of hard and anticorrosive coating on carbon steel. *Corros. Sci.*, 111523.
- Vovchenko, L., et al., 2023. Face-centered cubic packing model for microwave properties of polymer composites with segregated conductive network. *MRS Commun.* 1–7.
- Wang, X., et al., 2018. Graphene reinforced composites as protective coatings for oil and gas pipelines. *Nanomaterials* 8 (12), 1005.
- Wang, S., et al., 2021. Graphene/nanorubber reinforced electrically conductive epoxy composites with enhanced toughness. *J. Appl. Polym. Sci.* 138 (14), 50163.
- Wei, H., et al., 2020. Adhesion and cohesion of epoxy-based industrial composite coatings. *Compos. B Eng.* 193, 108035.
- Xavier, J.R., 2023. Multifunctional nanocomposite coatings for superior anticorrosive, flame retardant and mechanical properties in aerospace components. *Surf. Interfaces* 38, 102832.
- Xavier, J.R., Beryl, J.R., Vinodhini, S., 2021. Novel multifunctional nanocomposites for superior barrier, hydrophobic and mechanical properties of Mg alloy in marine environment. *Surf. Coat. Technol.* 421, 127475.
- Xiong, G., et al., 2019. Improved adhesion, heat resistance, anticorrosion properties of epoxy resins/POSS/methyl phenyl silicone coatings. *Prog. Org. Coat.* 135, 454–464.
- Yahya, M.N., et al., 2023. Modified locally derived graphene nanoplatelets for enhanced rheological, filtration and lubricity characteristics of water-based drilling fluids. *Arab. J. Chem.*, 105305.
- Yarahmadi, E., et al., 2018. Development and curing potential of epoxy/starch-functionalized graphene oxide nanocomposite coatings. *Prog. Org. Coat.* 119, 194–202.
- Ying, Y., et al., 2020. Micelles-based self-healing coating for improved protection of metal. *Arab. J. Chem.* 13 (1), 3137–3148.
- Zehra, S., Mobin, M., Aslam, R., 2023. Nanocontainers: A comprehensive review on their application in the stimuli-responsive smart functional coatings. *Prog. Org. Coat.* 176, 107389.
- Zhang, Z.-Q., et al., 2021. Corrosion resistance and superhydrophobicity of one-step polypropylene coating on anodized AZ31 Mg alloy. *J. Magnesium Alloys* 9 (4), 1443–1457.
- Zhang, R., et al., 2021. The role of graphene in anti-corrosion coatings: A review. *Constr. Build. Mater.* 294, 123613.
- Zhang, W., et al., 2021. Aerobic granular sludge (AGS) scouring to mitigate membrane fouling: performance, hydrodynamic mechanism and contribution quantification model. *Water Res.* 188, 116518.
- Zhang, F., et al., 2022. Recent advances on graphene: Synthesis, properties and applications. *Compos. A Appl. Sci. Manuf.* 160, 107051.
- Zhang, Y., et al., 2022. Graphene-like two-dimensional nanosheets-based anticorrosive coatings: A review. *J. Mater. Sci. Technol.* 129, 139–162.
- Zhang, Y., et al., 2023. Preparation of polyaniline encapsulated acrylic resin microcapsules and its active corrosion protection of coating for magnesium alloy. *Arab. J. Chem.* 16 (10), 105129.
- Zhang, W., Liang, W., Zhang, Z., 2022. Dynamic scouring of multifunctional granular material enhances filtration performance in membrane bioreactor: Mechanism and modeling. *J. Membr. Sci.* 663, 120979.
- Zhou, M., et al., 2013. Few-layer graphene obtained by electrochemical exfoliation of graphite cathode. *Chem. Phys. Lett.* 572, 61–65.
- Zhu, G., et al., 2023. Constructing a robust ZIF-7 based superhydrophobic coating with the excellent performance in self-cleaning, anti-icing, anti-biofouling and anti-corrosion. *Appl. Surf. Sci.* 622, 156907.